Copy

328

RESEARCH MEMORANDUM

TRANSONIC FLUTTER INVESTIGATION OF MODELS OF THE

SWEPTBACK WING OF A FIGHTER AIRPLANE

By Samuel L. Smith III and Robert W. Boswinkle, Jr.

Langley Aeronautical Laboratory
Langley Field, Va.

NATIONAL ADVISORY COMMITTEE
FOR AERONAUTICS
WASHINGTON
April 15, 1958

NATIONAL ADVISORY COMMITTEE FOR AERONAUTICS

RESEARCH MEMORANDUM

TRANSONIC FLUTTER INVESTIGATION OF MODELS OF THE

SWEPTBACK WING OF A FIGHTER AIRPLANE

By Samuel L. Smith III and Robert W. Boswinkle, Jr.

SUMMARY

A transonic flutter investigation has been made of models of the wing of a current fighter airplane. The models were dynamically and elastically scaled in accordance with criteria which include a flutter safety margin. The wings had an aspect ratio of 3.42 and were swept back 41.1° along the leading edge and 19.3° along the outer part of the trailing edge. A large trailing-edge fillet extended out to 50 percent of the semispan. The investigation was made in the Langley transonic blowdown tunnel and covered a Mach number range from 0.75 to 1.32.

The flutter boundary was located at simulated altitudes below sea level, the models being flutter free at altitudes above sea level. However, a region in which the models exhibited large responses to the turbulence of the tunnel stream extended to altitudes above sea level at supersonic Mach numbers. The significance with regard to the airplane of the large responses of the models is not known. The flutter boundary shifted to higher altitudes but remained below sea level with the addition of 15-percent-chord leading-edge extensions over the outer 35 percent of the semispan.

INTRODUCTION

The flutter characteristics of the wing of a current fighter airplane have been under study. The wing is swept back 41.1° along the leading edge and 19.3° along the outer part of the trailing edge. A large trailing-edge fillet extends out to 50 percent of the semispan. Calculations indicated that flutter would result at transonic speeds at sea level if the stiffness were reduced only slightly. Experimental data on similar wings (refs. 1 to 4) indicated that possibly a sufficient

stiffness margin existed; however, it was felt that the wing in question was sufficiently different from those of the references to warrant a separate experimental study.

The investigation was made in the Langley transonic blowdown tunnel with models which were dynamically and elastically scaled in accordance with criteria which include a flutter safety margin. The wing spar was cantilever-mounted inboard of the wing root and the tests were made at Mach numbers from 0.75 to 1.32 and at simulated altitudes extending to below sea level. The effect of installing a 15-percent-chord leading-edge extension over the outer 35 percent of the semispan was also investigated.

SYMBOLS

b   typical wing semichord, ft

c   local streamwise chord, ft

l length scale factor, $\dfrac{\text{Typical model length}}{\text{Corresponding airplane length}}$

m   mass scale factor, $\dfrac{\text{Typical model mass}}{\text{Corresponding airplane mass}}$

m'   mass of exposed panel, slugs

M   Mach number

q   dynamic pressure, lb/sq ft

s   value of y at wing tip

t   time scale factor, $\dfrac{\text{Time required for tunnel airstream to move 1 model chord length}}{\text{Time required for airplane to move 1 airplane chord length}}$

T   static temperature, $^{\circ}R$

$$v = \frac{\pi}{4} \int_{0}^{s} c^{2}\, dy$$

V   velocity, ft/sec

$\overline{V}$ reduced velocity based on a representative natural frequency, $V/b\omega_i$

y   distance from wing root measured perpendicular to wing root, ft

X,Y   streamwise and spanwise coordinates, respectively, defined in figure 4

η stiffness reduction factor used to provide margin of safety in application of model flutter-test results to the airplane

μ mass ratio, $m'/\rho v$

ρ static air density, slugs/cu ft

ω_i representative natural frequency, radians/sec

Subscripts:

A   airplane

M   model

MODELS

Geometry

The models were 3.125-percent-size versions of the wings of a current fighter airplane. The wing models had an aspect ratio of 3.42 and were swept back 41.1° along the leading edge and 19.3° along the outer part of the trailing edge. A large fillet at the trailing edge extended out to 50 percent of the semispan. A sketch of the model is given in figure 1 and some of the more important geometric properties are listed in table I. The fact that the plan-form aspect ratio is twice the exposed-panel aspect ratio (table I) is coincidental.

Because of damage to the models at flutter, six models were required in the investigation. Three models (designated wings 1 to 3) were without leading-edge chord-extensions and were intended to be identical. The other three models (designated wings 4 to 6) had leading-edge chord-extensions and were intended to be identical. In addition, the only intended differences between the two sets of models were differences caused by the addition of the leading-edge chord-extensions. Small differences between models 1 to 3 and also between models 4 to 6

did exist, as evidenced by the measured natural vibration frequencies and node lines (presented in the section entitled "Physical Properties").

The chord-extensions were over the outer 35 percent of the semi-span and increased the local wing chords by 15 percent. A model with leading-edge chord-extensions is shown mounted in the fuselage mounting block in figure 2. (As shown in figure 2, the wings were painted at intervals along the leading edge to aid in observing the motion of the models during the flutter runs.) The wings without leading-edge chord-extensions had a small amount of positive camber and the leading-edge chord-extensions of models 4 to 6 accentuated the camber.

Scaling

The nondimensional mass and stiffness distributions were required to be the same for the model as for the airplane. The mass and stiff-ness levels for the model were obtained by specifying the scale factors for the fundamental quantities involved: length, mass, and time.

The size of the model was limited by tunnel-wall-interference effects, and on the basis of past experience the length scale factor was chosen to be

$$l = 0.03125 \tag{1}$$

The mass scale factor was obtained from a requirement that the mass ratio μ should be the same for the model as for the airplane, which results in

$$m = \frac{\rho_M}{\rho_A} l^3 \tag{2}$$

In order to locate the simulated sea level near the middle of the tunnel density range available at a Mach number of 1, the density ratio was chosen to be $\rho_M/\rho_A = 1.97$. This location of simulated sea level allows altitudes below sea level to be obtained and flutter margins to be indicated for cases where flutter does not occur above sea level.

The time scale factor was obtained from a requirement that the reduced velocity $\overline{V}$ should be the same for the model as for the air-plane, which results in

$$t = \left(\frac{V_M}{V_A}\right)^{-1} l$$

Since the Mach number is the same for the model as for the airplane, the time scale factor may be written

$$t = \left(\frac{T_M}{T_A}\right)^{-1/2} l \qquad (3)$$

The static temperature for the airplane T_A is a function of altitude only, and for sea level it was taken to be 519° R. However, in the tunnel during a run, the temperature continually drops as air is expended from the reservoir and the temperatures obtained at the various flutter points during an investigation are different. A study of previous flutter data indicated that 408° R was near the average value of the static temperature that would be expected during the present runs, and this value was used to obtain the temperature ratio used in the scaling: $T_M/T_A = 0.786$.

A list of the pertinent wing and flow quantities and the design scale factors used is given in table II. It may be noted that the factor η is used in the scale factors for some of the quantities listed. The factor η has the value 0.76 and occurs because the stiffnesses of the models were made 76 percent of those which would result from application of the scale factors as specified (eqs. (1), (2), and (3)). The purpose of reducing the model stiffnesses was to provide a margin of safety in the application of the model flutter-test results to the airplane. Thus the design reduced velocity for the model is equal, not to that of the airplane, but to that of an airplane having stiffnesses 76 percent of those of the actual airplane.

The dynamic pressure and Mach number are quantities which are controllable during a run, whereas the temperature is not. If the dynamic pressure and Mach number are considered to be fixed and a static temperature different from the design value is obtained, both the density and velocity will be different from the values considered in the scaling. The density and velocity changes result, respectively, in values of mass ratio and reduced velocity different from the design values. However, a combination of reduced velocity and mass ratio which can be expressed in terms of the dynamic pressure

$$\frac{\overline{V}_M{}^2}{\mu_M} \propto q_M$$

is independent of the temperature, and this combination is exactly simulated in the runs by the expedient of interpreting the simulated altitude in terms of dynamic pressure. Thus, the scale factor in table II for dynamic pressure is used to convert the dynamic pressure for the airplane at any altitude and Mach number to the dynamic pressure for the model at the same altitude and Mach number. The dynamic pressure for the airplane is assumed to be that calculated by use of the ICAO standard atmosphere (ref. 5). It may be noted that, for a given altitude, q/M^2 is a constant.

The effect of not having the mass ratio and reduced velocity of the models exactly equal to those of the airplane is believed to be negligible in the present investigation. Experience with a wide variety of flutter models has indicated that, at least within the operational limits of the tunnel, flutter at a given Mach number tends to occur at a constant value of dynamic pressure regardless of the individual values of density and velocity.

Construction

The construction of the models is indicated in figure 1. The main spar was made of aluminum alloy, and aluminum-alloy ribs having U-shaped cross sections were welded to the main spar. The leading and trailing edges were of pine. Balsa was used to fill the wing to contour. Lead weights were placed in the wing at various locations and the wings were wrapped with silk cloth and painted. Each wing panel was instrumented with strain gages on the main spar near the root. The main spar was clamped inboard of the root, as shown in figure 1, and thus allowed some root flexibility. The mounting block shown in figure 2 was made of aluminum alloy.

Physical Properties

The first several natural cantilever frequencies and node lines of each of the six wings are given in figure 3. In obtaining the data an electromagnetic shaker was used to excite each panel separately. The shaker stem acted on the extended wing spars at the locations indicated by x in figure 3 and the spars were clamped as indicated in figure 1. The positions of the node lines were indicated by salt crystals sprinkled on the wings.

The right panel of model 2, which survived the flutter tests undamaged, was used to obtain the flexibility influence coefficients. Influence coefficients were obtained at 22 stations (fig. 4) on the wing by the method described in reference 6. The influence-coefficient matrix is given in table III. This matrix has been made symmetrical in table IV by taking the average of each pair of coefficients symmetric to the diagonal. The deviation of the coefficients in table III from the average values in table IV gives some indication of the accuracy of the measurements. Only 2.6 percent of the coefficients deviate more than 2 percent, and the greatest deviation is 3.6 percent.

The right panel of model 2 was cut into strips and the center of gravity, mass, and moment of inertia about the center of gravity of each strip were measured. The data are given in figure 5. Each strip was then cut as shown in figure 4 so that each section corresponded to one of the influence coefficient stations. The mass and center of gravity of each section were measured and the values are listed in figure 4. The masses given in figures 4 and 5 for the sections and strips include an allowance for the material lost in the saw cuts.

APPARATUS AND TESTS

The investigation was made in the Langley transonic blowdown tunnel, which has a slotted test section. The test section is octagonal in cross section and measures 26 inches between flats. During the operation of the tunnel, a preselected Mach number is set by means of a variable orifice downstream of the test section, and this Mach number is held approximately constant (after the orifice is choked) while the stagnation pressure, and thus the density, is increased. The static density range is approximately 0.001 to 0.012 slug per cubic foot, and Mach numbers from subsonic values to a maximum of about 1.4 may be obtained. Because of the expansion of the air in the reservoir during a run, the stagnation temperature continually decreases, and therefore the test-section velocity is not uniquely defined by the Mach number. Additional details of the tunnel are contained in reference 1. Excellent agreement between flutter data obtained in the tunnel and in free air has been observed (ref. 7).

In the investigation, each model was cantilever-mounted in the mounting block shown in figure 2. The mounting block was fitted into a sting in such a way as to form a fuselage 3 inches in diameter which extended upstream into the subsonic flow region of the tunnel. This arrangement prevented the formation of shock waves from the fuselage nose which might reflect from the tunnel walls onto the model. A sketch of the model mounted on the sting and installed in the tunnel is shown in figure 6. The sting and model weighed approximately

290 pounds and the system had a fundamental bending frequency of about 15 cycles per second.

Wire strain gages were mounted on the wing spars near the root and were oriented so as to indicate model deflections about two different axes. The strain-gage signals, the tunnel stagnation and static pressures, and the stagnation temperature were recorded on a recording oscillograph. The strain-gage signals were used to indicate the start of flutter and the flutter frequency. High-speed motion pictures were made during some of the runs.

The wings without leading-edge chord-extensions were tested at zero angle of attack. The wings with leading-edge chord-extensions were tested at -2^O angle of attack in an attempt to reduce the static loads.

RESULTS AND DISCUSSION

Presentation of Data

The results of the investigation are given in table V(a) for the wings without leading-edge chord-extensions and in table V(b) for the wings with leading-edge chord-extensions. The dynamic pressure at the various test points is plotted as a function of Mach number in figure 7 for the wings without leading-edge chord-extensions and in figure 8 for the wings with leading-edge chord-extensions. Lines of constant simulated altitude are also indicated in figures 7 and 8.

Each circle symbol in figures 7 and 8 indicates the point of the start of definite flutter and each square symbol indicates the point of the maximum dynamic pressure attained during a run without obtaining flutter. A dashed line below a symbol defines a low-damping condition. In the low-damping condition, the strain-gage records and the motion pictures indicated periods of nearly sinusoidal, lowly damped oscillations. The point for the beginning of low damping in each run was indefinite and was somewhat arbitrarily chosen. On the other hand, the point for the beginning of flutter in each run in which flutter was obtained was definite and was characterized by rapidly diverging oscillations. The low-damping region is indicated for the wings without leading-edge chord-extensions in figure 7 by dotted shading.

The response frequencies of the wings are indicated near most of the data points in figures 7 and 8. The response frequency for no-flutter or low-damping points was taken as the predominant oscillation frequency of the models; at flutter, of course, the flutter frequency is listed.

The flutter mode for both configurations investigated involved bending and torsion of the wing with some rotation in pitch at the wing root. The rotation in pitch of the wing root was possible because, as previously noted, the main spar was clamped inboard of the root. A typical oscillograph record showing the strain-gage traces during low damping and flutter is given in figure 9.

Interpretation of Results

As stated in the section entitled "Scaling," the stiffnesses of models were 76 percent of the scaled airplane stiffnesses. The simulated altitudes indicated in figures 7 and 8 are thus to be interpreted as altitudes which, if cleared by the model, could be reached with a 32-percent $(1/0.76 = 1.32)$ margin of safety in stiffness by the airplane. This statement assumes, of course, that in all other respects the model exactly simulates the airplane.

An alternate interpretation of the results arises from the fact that for most configurations the dynamic pressure required for flutter varies, to a first approximation, directly with the stiffness level. Thus, a flutter point obtained with the model indicates that the airplane will flutter at the same Mach number at a simulated altitude corresponding to a dynamic pressure 32 percent higher than that for the model.

Wings Without Leading-Edge Chord-Extensions

The transonic flutter boundary for the models of the wing without leading-edge chord-extensions is located at altitudes below sea level (fig. 7). The dynamic pressure for flutter is indicated to be a minimum at a Mach number of about 0.87. The low-damping region extends at supersonic Mach numbers to altitudes above sea level. With regard to the airplane, the significance of the low damping obtained with the models is not known. Photographs of the wings without leading-edge chord-extensions after flutter are given in figures 10(a) to 10(c).

Wings With Leading-Edge Chord-Extensions

Because of various data-recording difficulties, the flutter points at the three lowest Mach numbers for the wings with leading-edge extensions (fig. 8) are known only to an estimated accuracy of ±100 lb/sq ft for dynamic pressure and ±0.03 for Mach number. However, the shape of the transonic flutter boundary is shown to be similar to that for the wings without leading-edge chord-extensions (fig. 7). Although the
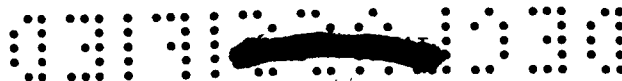
flutter boundary shifted to higher altitudes with the addition of the leading-edge chord-extensions, no flutter was obtained at altitudes above sea level.

Low damping preceded the flutter points at the lowest Mach numbers, but the location of these points could not be ascertained and they are omitted in figure 8 and table V(b). A photograph of one of the wings with leading-edge chord-extensions after flutter is given in figure 10(d).

CONCLUSIONS

The transonic flutter characteristics of models of the sweptback wing of a current fighter airplane have been studied in the Langley transonic blowdown tunnel. The models were dynamically and elastically scaled in accordance with criteria which include a flutter safety margin. The scaling was such that if at a given Mach number a certain altitude is cleared by the model, that Mach number and altitude could be reached with a 32 percent margin of safety in stiffness by the airplane. The following results were obtained:

1. Although the flutter boundary for the wings without leading-edge chord-extensions was located at altitudes below sea level, a region of lowly damped oscillations that extended to altitudes above sea level was obtained at supersonic Mach numbers.

2. With the addition of 15-percent-chord leading-edge extensions over the outer 35 percent of the semispan, the flutter boundary shifted to higher altitudes but remained below sea level.

Langley Aeronautical Laboratory,
    National Advisory Committee for Aeronautics,
        Langley Field, Va., December 20, 1957.

REFERENCES

1. Unangst, John R., and Jones, George W., Jr.: Some Effects of Sweep and Aspect Ratio on the Transonic Flutter Characteristics of a Series of Thin Cantilever Wings Having a Taper Ratio of 0.6. NACA RM L55I13a, 1956.

2. Jones, George W., Jr., and Unangst, John R.: Investigation To Determine Effects of Center-of-Gravity Location on Transonic Flutter Characteristics of a 45° Sweptback Wing. NACA RM L55K30, 1956.

3. Ruhlin, Charles L.: Experimental Transonic Flutter Characteristics of an Untapered, 45° Sweptback, Aspect-Ratio-4 Wing. NACA RM L55L22, 1956.

4. Land, Norman S., and Abbott, Frank T., Jr.: Transonic Flutter Investigation of a Fighter-Airplane Wing Model and Comparison With a Systematic Plan-Form Series. NACA RM L55B16, 1955.

5. Anon.: Standard Atmosphere - Tables and Data for Altitudes to 65,800 Feet. NACA Rep. 1235, 1955. (Supersedes NACA TN 3182.)

6. Jones, George W., Jr., and Young, Lou S., Jr.: Transonic Flutter Investigation of Two 64° Delta Wings With Simulated Streamwise Rib and Orthogonal Spar Construction. NACA RM L56I27, 1957.

7. Bursnall, William J.: Initial Flutter Tests in the Langley Transonic Blowdown Tunnel and Comparison With Free-Flight Flutter Results. NACA RM L52K14, 1953.

TABLE I.- GEOMETRY OF MODELS WITHOUT

LEADING-EDGE CHORD-EXTENSIONS

Streamwise airfoil section, tip . . . .   Modified NACA 65A006
Streamwise airfoil section, root . . . .   Modified NACA 65A007
Leading-edge sweepback, deg 41.1
Trailing-edge sweepback, deg 19.3
Span, ft 1.252
Plan-form area based on extension of panels
  to model center line, sq ft 0.4582
Plan-form aspect ratio based on extension of
  panels to model center line 3.42
Fuselage diameter, ft 0.250
Exposed-panel span, ft 0.498
Exposed-panel area, sq ft 0.1453
Exposed-panel aspect ratio 1.71

TABLE II.- DESIGN SCALE FACTORS OF PERTINENT

WING AND FLOW QUANTITIES

$$\left[\frac{\rho_M}{\rho_A} = 1.97; \quad \frac{T_M}{T_A} = 0.786; \quad \eta = 0.76\right]$$

Quantity	Design scale factor	
	Symbolical	Numerical
Fundamental quantities:		
Length	l	0.03125
Mass	$m = \dfrac{\rho_M}{\rho_A} l^3$	0.6012×10^{-4}
Time	$t = \left(\dfrac{T_M}{T_A}\right)^{-1/2} l$	0.03525
Derived quantities:		
Stream velocity	$l t^{-1}$	0.886
Stream dynamic pressure	$m l^{-1} t^{-2}$	1.548
Moment of inertia	$m l^2$	0.587×10^{-7}
Flexibility influence coefficients .	$\eta^{-1} m^{-1} t^2$	27.195
Natural vibration frequencies . . .	$\eta^{1/2} t^{-1}$	24.73
Bending and torsional stiffnesses .	$\eta l^3 m t^{-2}$	1.122×10^{-6}

TABLE III.- FLEXIBILITY INFLUENCE COEFFICIENTS ON RIGHT

PANEL OF WING 2.   UNITS ARE $\frac{in.}{lb} \times 10^5$

Deflection point	Load point																					
	1	2	3	4	5	6	7	8	9	10	11	12	13	14	15	16	17	18	19	20	21	22
1	85.0	76.0	64.1	66.7	76.1	81.1	24.9	26.9	37.8	45.9	54.4	61.1	-11.7	0	10.7	22.7	32.5	40.0	-45.7	-22.3	-65.1	12.3
2	76.2	122	160	190	236	264	58.0	101	140	190	227	256	45.1	80.3	124	169	214	267	25.3	74.1	16.3	16.5
3	63.7	157	319	346	398	490	74.2	142	247	340	400	506	91.4	170	241	352	429	490	92.2	158	90.5	24.2
4	66.4	187	347	692	782	912	109	235	397	590	773	942	154	265	412	607	762	937	179	272	171	26.0
5	78.0	229	396	784	1,330	1,660	148	295	564	928	1,290	1,670	233	387	638	1,000	1,350	1,760	285	448	313	31.9
6	79.1	257	499	892	1,610	2,830	163	359	649	1,110	1,770	2,680	269	462	795	1,290	1,910	2,770	370	543	435	33.9
7	26.0	58.6	74.9	111	147	165	46.6	59.8	88.6	120	157	175	53.9	75.5	101	140	164	174	57.8	83.5	60.4	13.9
8	27.2	98.9	143	228	295	354	57.7	138	185	259	312	391	87.0	153	221	267	322	386	112	158	128	14.0
9	57.4	140	245	398	548	664	87.0	186	339	447	572	693	145	240	361	493	652	710	190	284	218	21.2
10	45.9	183	345	595	920	1,110	122	261	446	708	958	1,240	200	347	552	798	1,080	1,280	276	408	309	26.7
11	55.7	221	421	772	1,280	1,780	155	316	570	972	1,400	1,960	268	426	709	1,110	1,660	2,170	369	517	406	29.5
12	61.8	250	509	958	1,660	2,720	173	389	711	1,230	1,950	3,220	312	559	929	1,470	2,220	3,250	446	624	473	41.0
13	-11.6	45.5	90.9	152	231	262	54.1	88.4	143	199	274	306	148	170	205	277	308	335	194	215	239	10.8
14	0	79.4	171	272	385	471	73.5	153	249	352	443	555	171	303	359	447	531	601	278	365	308	15.4
15	11.5	122	241	420	628	796	102	230	364	552	716	924	211	356	613	697	851	998	323	463	381	22.0
16	22.9	173	331	609	1,000	1,290	142	267	494	814	1,130	1,460	273	447	695	1,200	1,410	1,730	392	505	447	25.2
17	32.7	208	430	777	1,340	1,950	169	337	655	1,120	1,660	2,250	308	549	841	1,410	1,980	2,520	439	636	540	27.1
18	39.1	270	496	934	1,760	2,770	172	385	703	1,270	2,160	3,250	337	605	966	1,730	2,520	4,170	476	682	584	40.4
19	-45.4	25.3	94.2	173	276	370	57.4	114	191	269	349	438	196	274	511	385	440	464	449	441	542	13.8
20	-22.8	75.4	156	274	432	538	81.9	161	287	399	498	601	218	358	459	507	636	680	440	723	552	11.8
21	-64.2	16.6	91.2	169	315	430	59.5	129	216	308	401	469	237	314	376	444	538	589	545	555	892	9.50
22	12.7	16.6	24.2	26.0	32.4	33.9	14.0	14.2	21.2	26.4	28.9	42.4	11.0	15.2	22.2	25.7	28.1	40.2	13.4	12.3	9.44	8.57

TABLE IV.- FLEXIBILITY INFLUENCE COEFFICIENTS OF TABLE III AFTER

BEING MADE SYMMETRICAL. UNITS ARE $\frac{in.}{lb} \times 10^5$

Deflection point	Load point																					
	1	2	3	4	5	6	7	8	9	10	11	12	13	14	15	16	17	18	19	20	21	22
1	85.0	76.1	63.9	66.6	77.0	80.1	25.4	27.0	37.6	45.9	55.0	61.4	-11.6	0	11.1	22.8	32.6	39.6	-45.6	-22.6	-64.6	12.5
2		122	158	188	232	260	58.3	100	140	186	224	253	45.3	79.8	123	171	211	268	25.3	74.8	16.4	16.6
3			319	346	397	494	74.6	142	246	342	410	508	91.2	170	241	332	430	493	93.2	157	90.8	24.2
4				692	785	902	110	230	398	592	772	950	153	268	416	608	770	936	176	273	170	26.0
5					1,330	1,640	148	295	556	924	1,280	1,660	232	385	633	1,000	1,340	1,760	280	440	314	32.2
6						2,830	164	356	656	1,110	1,780	2,700	266	466	796	1,290	1,930	2,770	370	540	432	33.9
7							46.6	58.8	87.8	121	156	174	54.0	74.5	102	141	166	173	57.6	82.7	60.0	14.0
8								138	186	260	314	390	87.7	153	226	267	330	386	113	160	128	14.1
9									359	446	571	702	144	244	362	494	654	706	190	286	217	21.2
10										708	965	1,240	200	350	552	806	1,100	1,280	272	404	308	26.6
11											1,400	1,960	271	434	712	1,120	1,660	2,160	359	508	404	29.2
12												3,220	309	557	926	1,460	2,240	3,250	442	612	471	41.7
13													148	170	208	275	308	335	195	216	238	10.9
14														303	358	447	540	602	276	362	311	15.3
15															613	696	846	982	317	461	378	22.1
16																1,200	1,410	1,730	388	506	446	25.4
17																	1,980	2,520	440	636	539	27.6
18																		4,170	470	681	586	40.3
19																			449	440	544	13.6
20																				723	554	12.0
21																					892	9.47
22																						8.57

TABLE V.- COMPILATION OF TEST RESULTS

Wing	Run	Point	Panel behavior* Left	Right	M	q, lb/sq ft	V, ft/sec	ρ, slugs/cu ft	T, $^{\circ}$R	Response frequency, cps Left	Right
(a) Wings without leading-edge chord-extensions											
1	1	a	Q	Q	0.877	1,921	889.1	0.0048	427.8	---	---
1	2	a	L	L	1.095	2,228	1,089.2	.0038	411.8	233	233
		b	Q	Q	1.099	2,795	1,070.8	.0049	395.1	260	250
1	3	a	L	L	1.312	3,264	1,243.0	.0042	373.6	260	260
		b	Q	Q	1.317	3,924	1,215.4	.0053	354.5	275	260
1	4	a	L	L	1.028	3,390	1,004.7	.0067	397.5	300	290
		b	F	L	1.022	3,622	988.1	.0074	389.0	310	310
3	5	a	L	L	1.211	2,821	1,174.9	.0041	391.8	260	265
		b	Q	Q	1.218	4,118	1,115.3	.0067	349.0	300	300
1	6	a	X	L	1.155	2,524	1,128.2	.0040	397.1	---	233
		b	X	Q	1.140	3,747	1,054.7	.0067	356.3	---	267
1	7	a	X	L	1.056	2,860	1,054.1	.0051	414.7	---	267
		b	X	Q	1.030	3,688	973.4	.0078	371.7	---	270
1	8	a	X	L	.755	2,435	783.2	.0079	447.8	---	300
		b	X	Q	.758	2,794	755.6	.0098	413.5	---	300
1	9	a	X	L	.863	2,086	905.0	.0051	457.7	---	250
		b	X	F	.870	2,418	906.3	.0059	451.6	---	262
3	10	a	L	X	.815	2,698	835.8	.0077	437.7	270	---
		b	F	X	.822	2,933	835.1	.0084	429.5	310	---
2	11	a	L	N	.898	1,971	895.7	.0049	414.0	265	---
		b	Q	Q	.888	2,205	877.2	.0057	406.1	270	250
2	12	a	Q	N	.979	2,773	946.6	.0062	389.1	280	---
2	13	a	L	N	.938	2,683	931.2	.0062	410.2	250	---
		b	F	N	.942	3,154	920.7	.0074	397.6	300	---
(b) Wings with leading-edge chord-extensions											
6	14	(†)	F	L	0.99	3,038	--------	-------	------	290	285
6	15	(†)	X	F	.82	2,419	--------	-------	------	---	---
5	16	a	L	X	1.086	3,240	1,042.2	0.0060	383.3	250	---
		b	F	X	1.086	3,802	1,014.0	.0074	362.8	300	---
4	17	(†)	F	F	.890	2,010	895.4	.0050	421.3	250	250

*Panel-behavior code: F - flutter; L - low damping; Q - maximum q, no flutter;
X - panel damaged; N - no flutter.

†Complete records were not obtained on these runs. The values given are estimates based on available information.
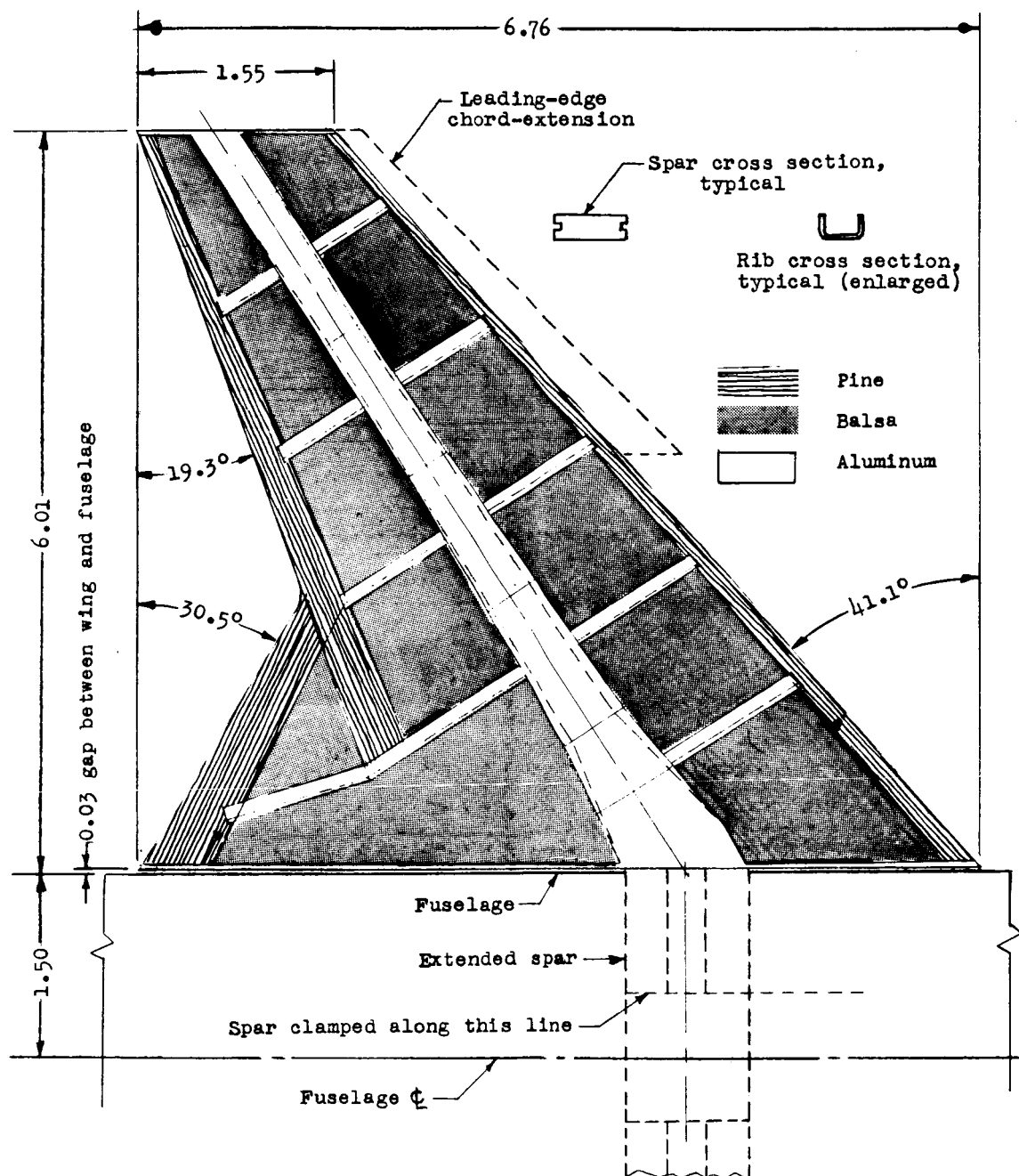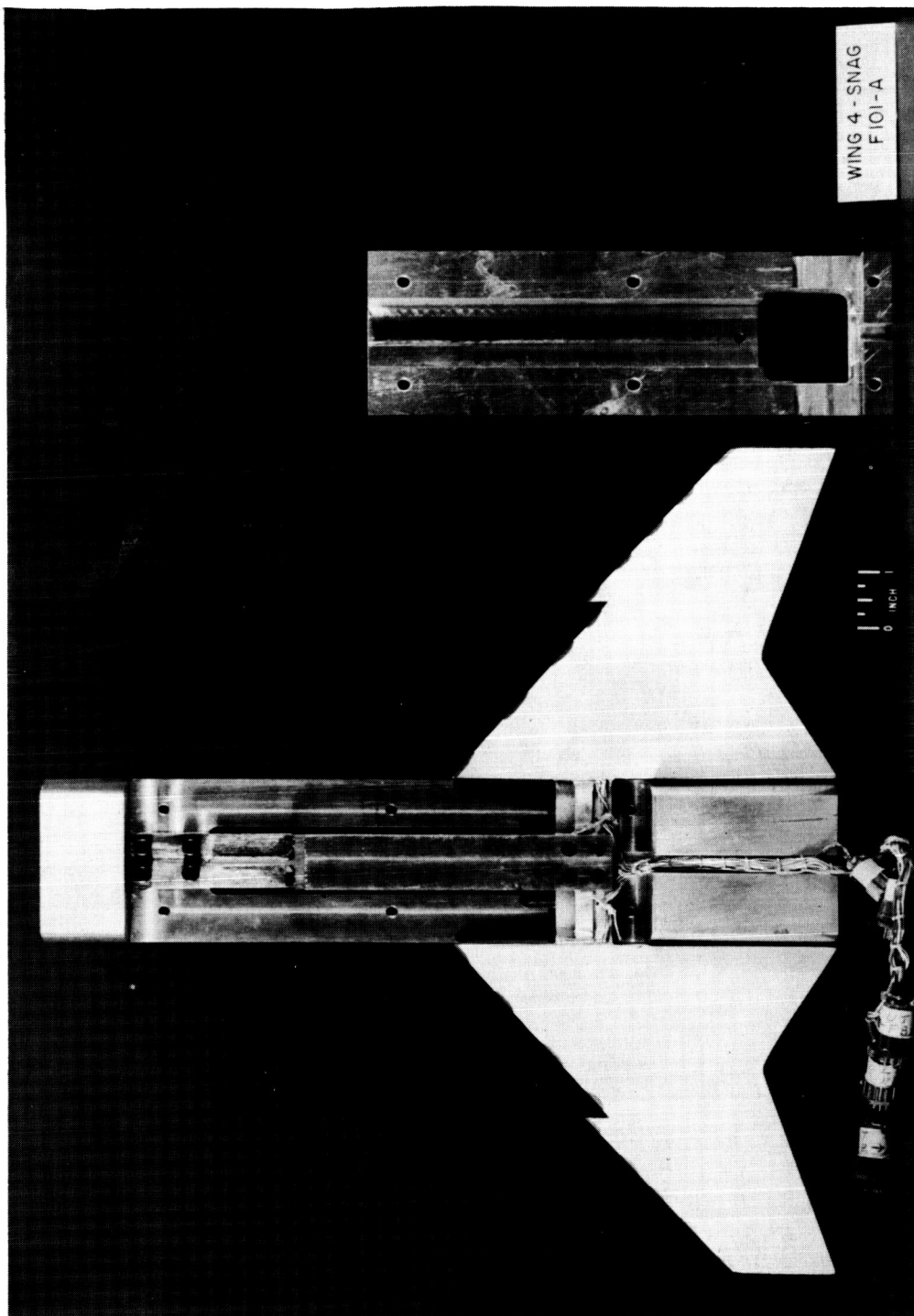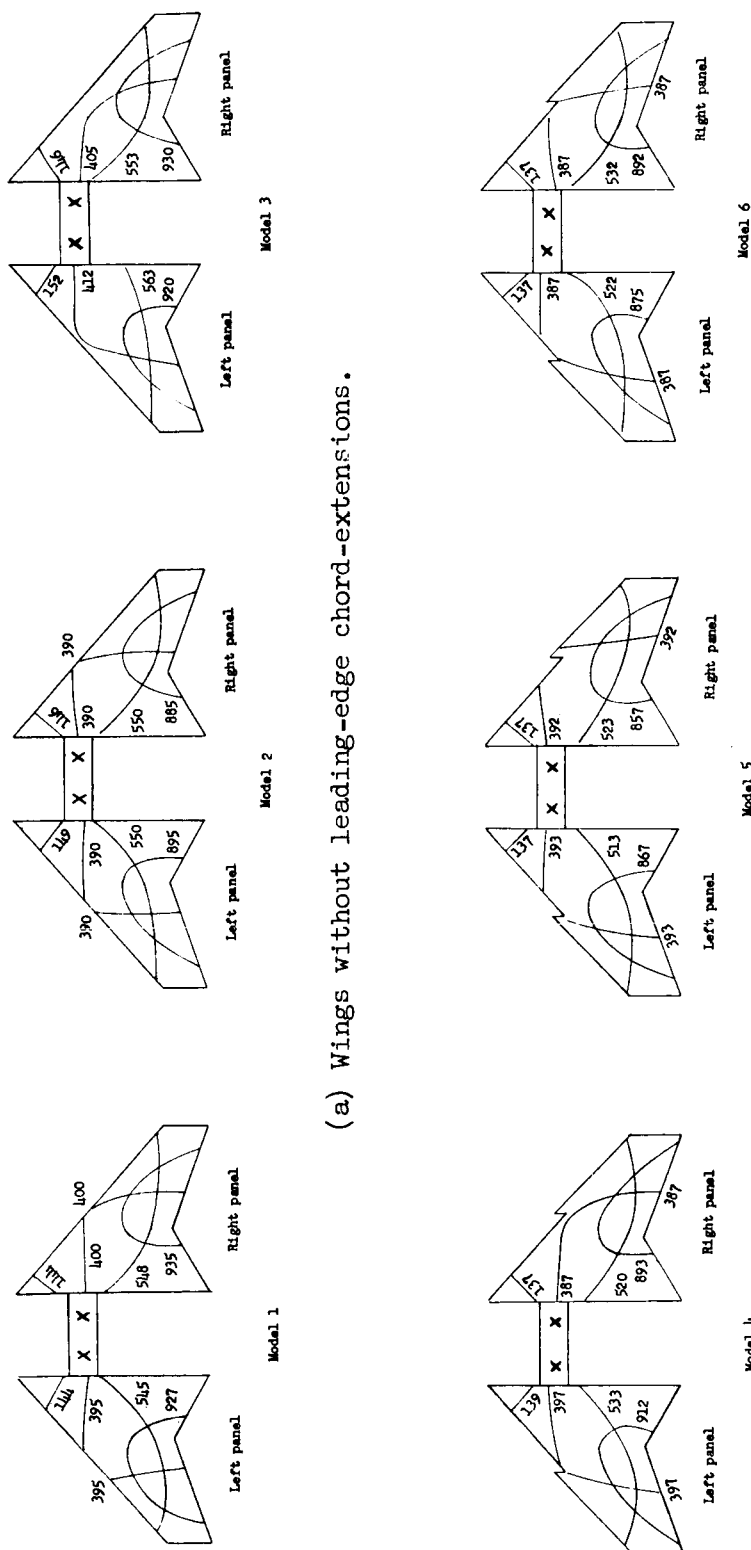
Figure 1.- Drawing of model. Lead weights are not indicated. Linear dimensions are in inches.

L-57-11

Figure 2.- Photograph of wing with leading-edge chord-extensions in mounting block. (Wings were painted at intervals along the leading edge.)

(a) Wings without leading-edge chord-extensions.

(b) Wings with leading-edge chord-extensions.

Figure 3.- Measured natural vibration frequencies and node lines. Symbol x indicates shaker location. Numbers beside node lines indicate frequencies in cycles per second.
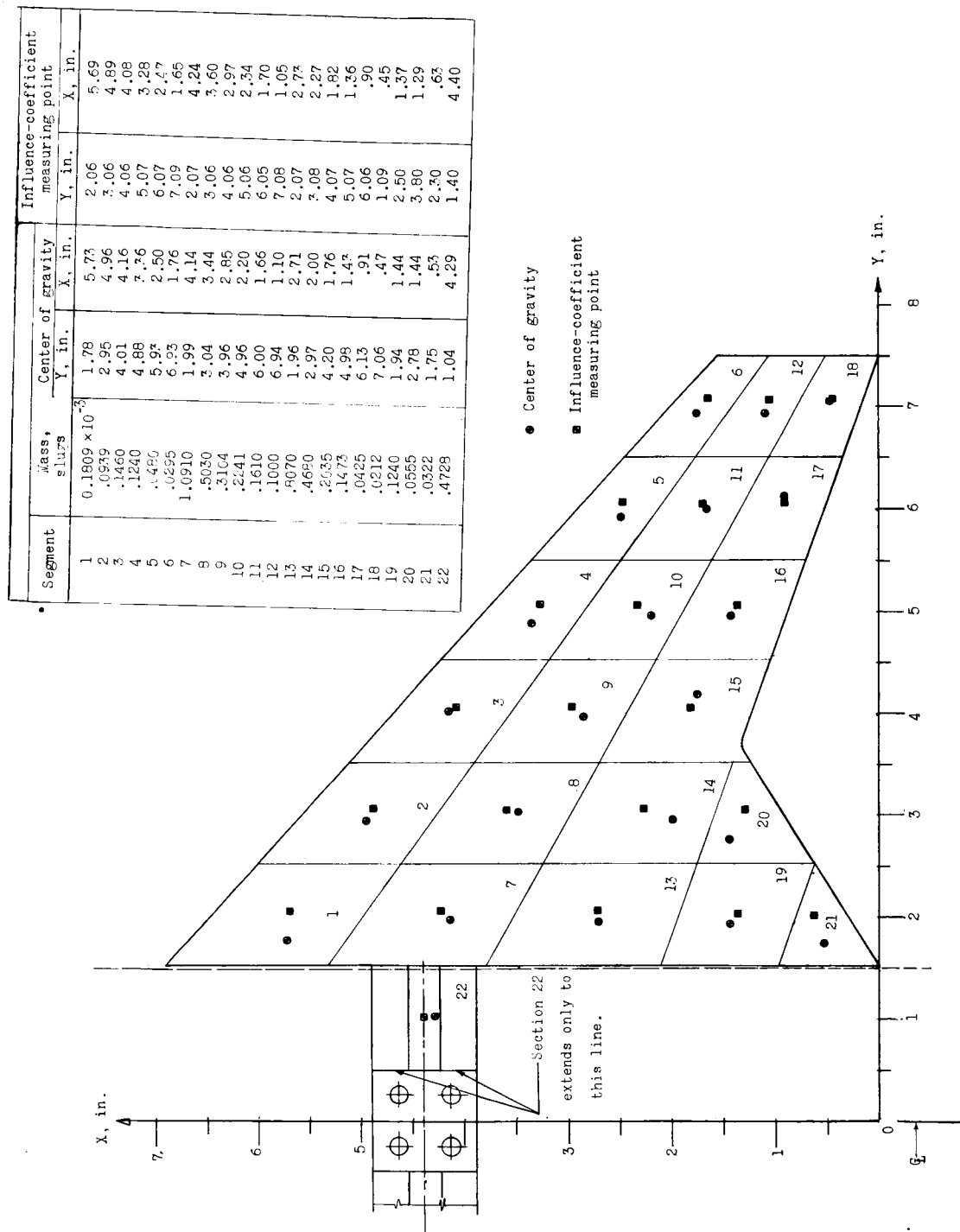
Segment	Mass, slugs	Center of gravity Y, in.	Center of gravity X, in.	Influence-coefficient measuring point Y, in.	Influence-coefficient measuring point X, in.
1	0.1809 ×10⁻³	1.78	5.73	2.06	5.69
2	.0939	2.95	4.96	3.06	4.89
3	.1460	4.01	4.16	4.06	4.08
4	.1240	4.88	3.36	5.07	3.28
5	.480	5.97	2.50	6.07	2.47
6	.0295	6.93	1.76	7.09	1.65
7	1.0910	1.99	4.14	2.07	4.24
8	.5030	3.04	3.44	3.06	3.60
9	.3164	3.96	2.85	4.06	2.97
10	.2241	4.96	2.20	5.06	2.34
11	.1610	6.00	1.66	6.05	1.70
12	.1000	6.94	1.10	7.08	1.05
13	.8070	1.96	2.71	2.07	2.73
14	.4660	2.97	2.00	3.07	2.27
15	.2035	4.20	1.76	4.07	1.82
16	.1473	4.98	1.43	5.07	1.36
17	.0425	6.13	.91	6.06	.90
18	.0212	7.06	.47	1.09	.45
19	.1240	1.94	1.44	2.50	1.37
20	.0555	2.78	1.44	3.80	1.29
21	.0322	1.75	.53	2.70	.63
22	.4728	1.04	4.29	1.40	4.40

Figure 4.- Sketch of wing without leading-edge chord-extensions, showing influence-coefficient station and center of gravity of various segments.
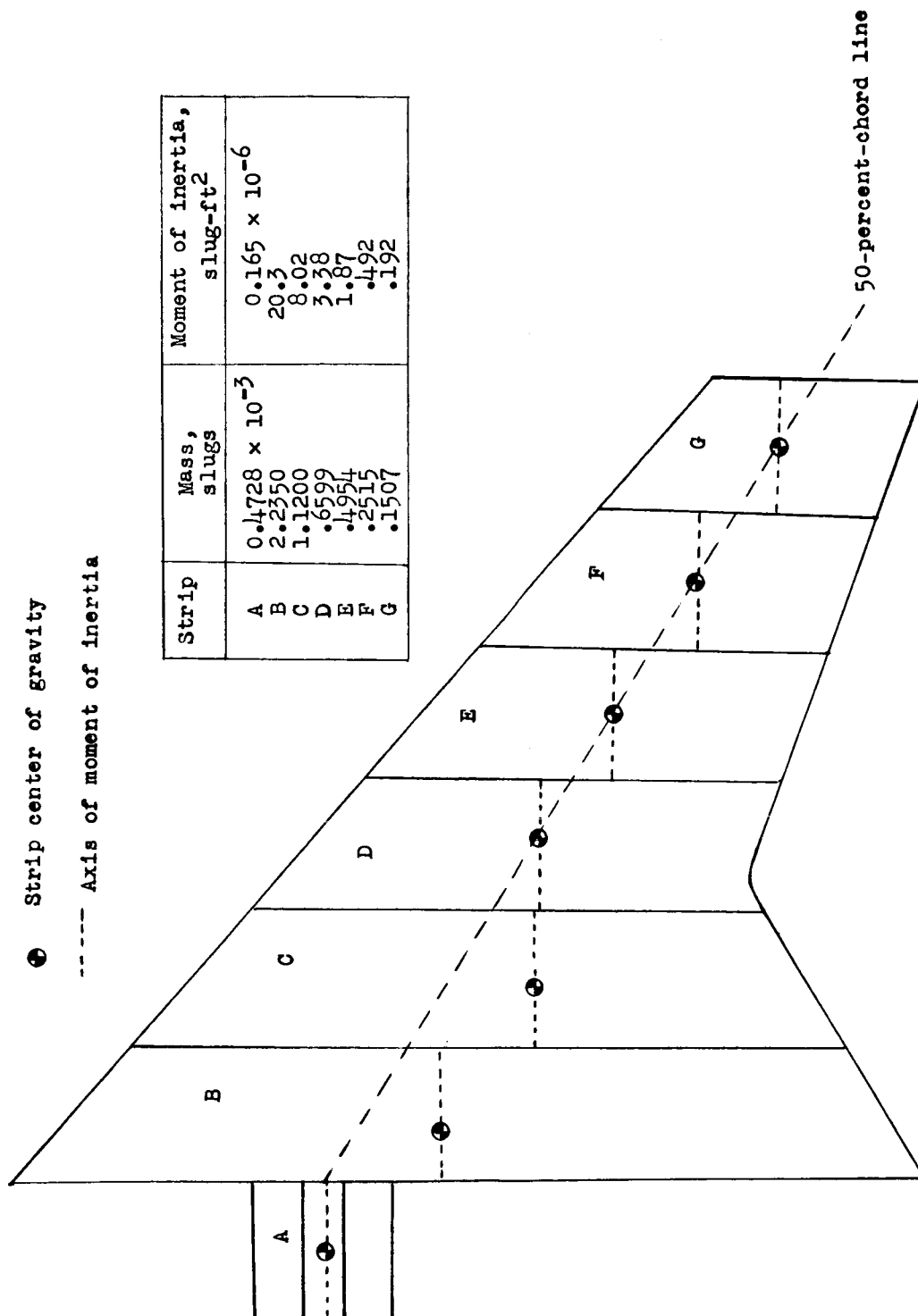
Strip	Mass, slugs	Moment of Inertia, slug-ft^2
A	0.4728×10^{-3}	0.165×10^{-6}
B	2.2350	20.3
C	1.1200	8.02
D	.6599	3.38
E	.4954	1.87
F	.2515	.492
G	.1507	.192

● Strip center of gravity

--- Axis of moment of inertia

--- 50-percent-chord line

A B C D E F G

Figure 5.- Sketch of wing without leading-edge chord-extensions showing strips and strip centers of gravity.

Sting support

Section A-A

A

A

$26\frac{1}{4}$ inches

Extension nose

Air flow

Support wires
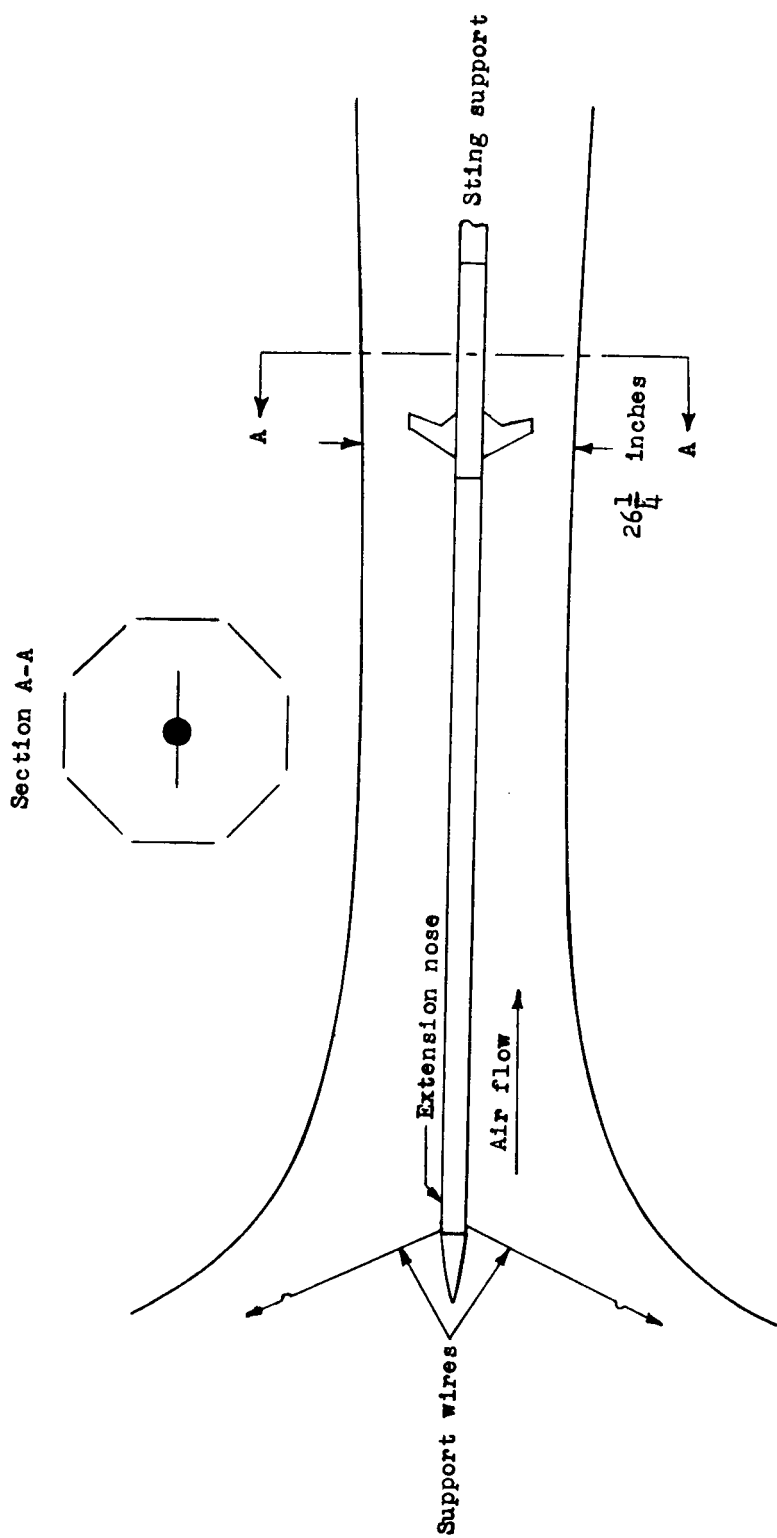
Figure 6.- Sketch of model in the Langley transonic blowdown tunnel.

Figure 7.- Transonic flutter characteristics of wings without leading-edge chord-extensions.

O   Definite start of flutter
ᠥ   Definite start of flutter; location
         of flutter point estimated
– – – Low-damping condition

Numbers beside data points indicate
response frequencies in cps.
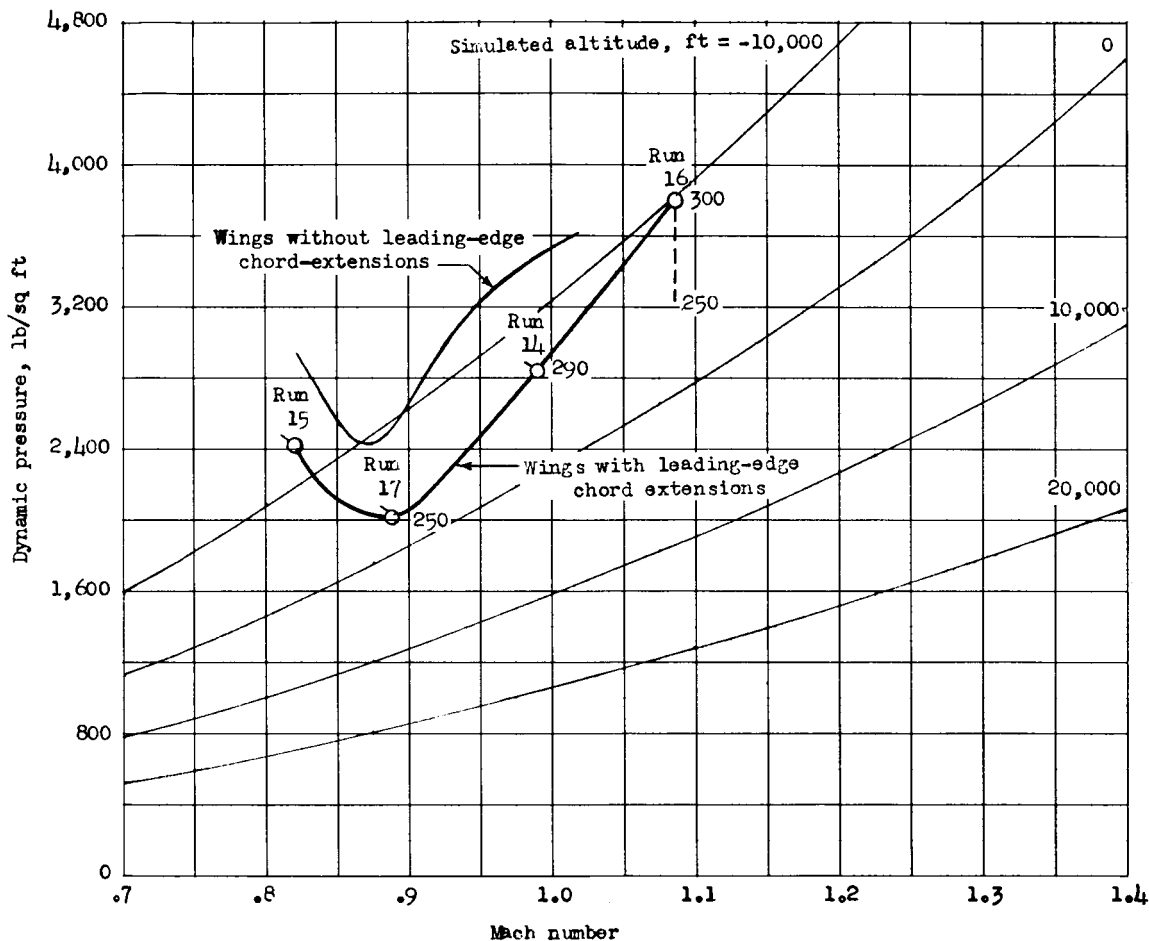
Figure 8.- Comparison of transonic flutter characteristics of wings with
    and without leading-edge chord-extensions. (For runs 14, 15, and 17
    the accuracy of the data is less than that for the other runs, and
    although low-damping conditions preceded flutter, they are not
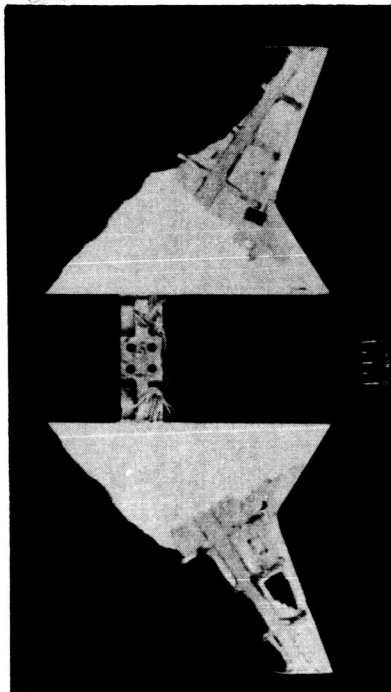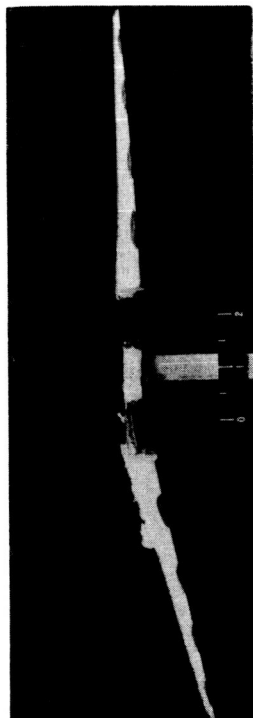   indicated here.)
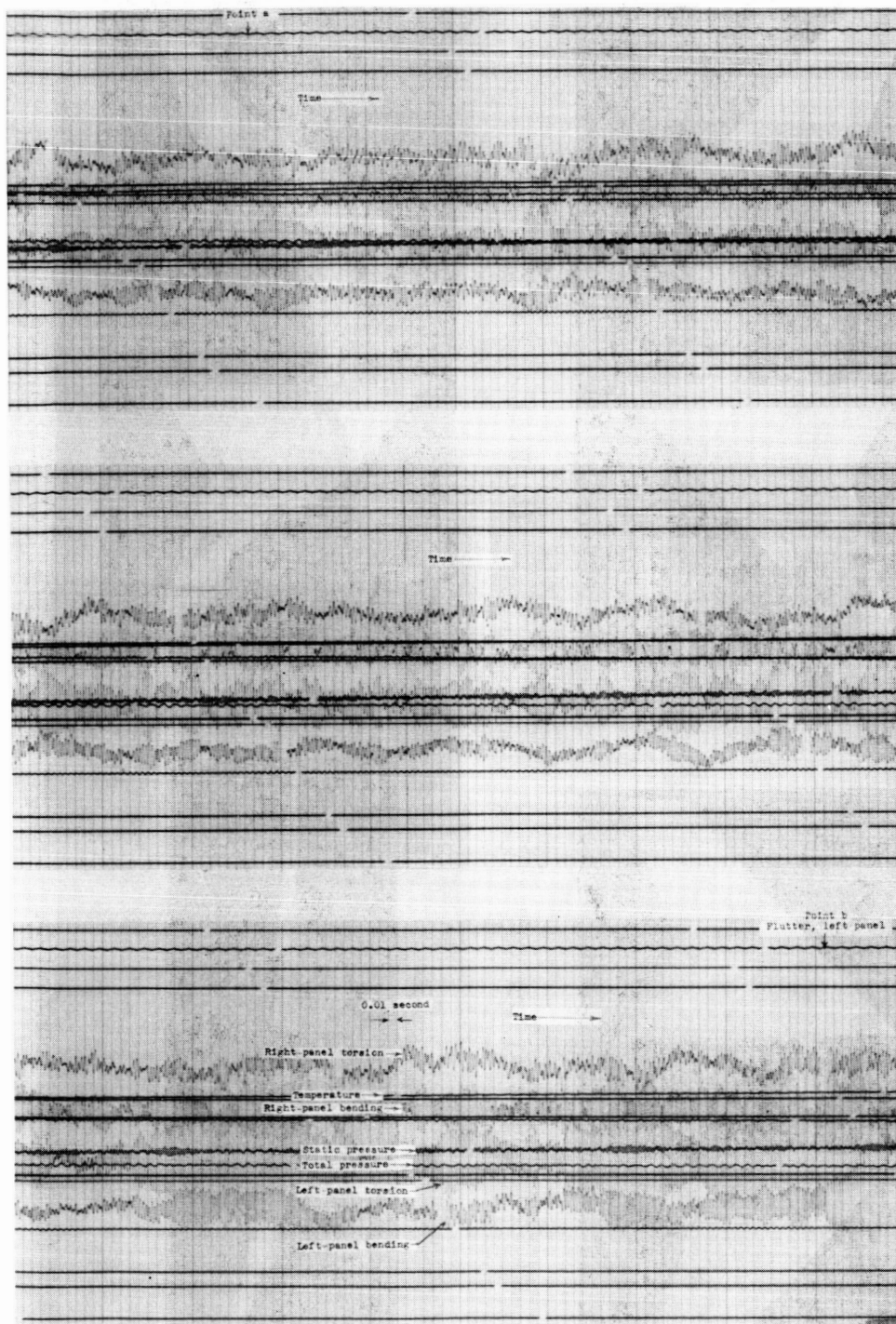
Figure 9.- A typical oscillograph record (run 4, wing 1).

CONFIDENTIAL
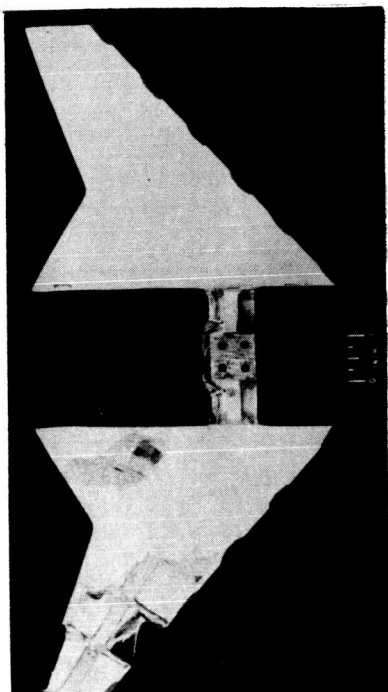
(b) Wing 2, bottom view.

(d) Wing 5, top view. L-57-5501

(a) Wing 1, top view.

(c) Wing 3, front view.

Figure 10.- Photographs of damaged models. (Wings were painted at intervals along the leading edge.)